International Journal of Innovative Computing, Information and Control
Volume **15**, Number **5**, October **2019**

ICIC International ©2019 ISSN 1349-4198
pp. **1793–1805**

SELECTIVE HARMONIC ELIMINATION PWM STRATEGY FOR THREE-LEVEL NPC INVERTERS UNDER FAULT-TOLERANT OPERATION

Bijun Dai[1], Ming Zhang[2], Yuanbo Guo[1] and Xiaohua Zhang[1,2]

[1]School of Electrical Engineering
Dalian University of Technology
No. 2, Linggong Rd., Ganjingzi Dist., Dalian 116024, P. R. China
guoyuanbo@163.com

[2]School of Electrical Engineering and Automation
Harbin Institute of Technology
No. 92, West Dazhi St., Nangang Dist., Harbin 150001, P. R. China
zmstc19719@126.com

Received December 2018; revised April 2019

Abstract. *To improve the reliability in high voltage and high power applications, the fault-tolerant control of three-level neutral-point-clamped (3L-NPC) inverter has been deeply studied. In this paper, the eight-switch three-phase inverter (ESTPI) is selected as the fault-tolerant topology of 3L-NPC inverter, and the synchronous modulation strategy of ESTPI is discussed for some particular application situation working at low switching frequency. The harmonic distribution of the ESTPI is analyzed firstly under synchronous modulation. To eliminate the specific low-order harmonics including the frequency tripling harmonics, the selective harmonic elimination pulse-width modulation (SHEPWM) based synchronous modulation strategy for the ESTPI is proposed in this paper, which can ensure a good performance of output voltage for 3L-NPC inverter under fault-tolerant operation. The effectiveness and feasibility of the proposed method are verified by the experimental results.*

Keywords: Three-level neutral-point-clamped inverter, Fault-tolerant operation, Synchronous modulation, Selective harmonic elimination pulse-width modulation

1. **Introduction.** The three-level neutral-point-clamped (3L-NPC) inverter has been widely used in high voltage and high power applications, such as the electric traction system, the variable frequency speed regulation system and the flexible AC transmission system. Considering the system reliability and safety, the fault-tolerant operation control of 3L-NPC inverter has become a hot topic in the multi-level inverter field [1,2].

The research of the fault-tolerant operation control for 3L-NPC inverter can be divided into two parts: the fault-tolerant topology research and the fault-tolerant modulation strategy research. The fault-tolerant modulation strategy should be studied based on the specific fault-tolerant topology. At present, the eight-switch three-phase inverter (ESTPI) is the most widely studied fault-tolerant topology of 3L-NPC inverter, for the advantages of using least additional power devices [3,4]. The fault-tolerant modulation strategy of the ESTPI currently focuses on the asynchronous modulation strategy (the carrier frequency f_s is constant while the modulation frequency f_c varies), such as space vector pulse-width modulation (SVPWM) and carrier-based pulse-width modulation (CBPWM) [5,6]. Moreover, SVPWM and CBPWM of the ESTPI can be demonstrated to be equivalent [7].

DOI: 10.24507/ijicic.15.05.1793

However, the asynchronous modulation strategy of the ESTPI is not applicable to the system asking for low switching frequency. To reduce the switching losses, the switching frequency of the 3L-NPC inverter in the electric traction system, for instance, is usually lower than 1 kHz. Figure 1 shows the multi-mode PWM strategy used in the electric traction system. In the low speed region and the high speed region, the modulation strategies of the inverter in electric traction system are asynchronous modulation and square wave modulation respectively. However, in the medium speed region, the piecewise-synchronous-modulation strategy is used instead of the asynchronous modulation strategy to achieve a better output voltage performance and a smoother transition with limited switching frequency. Obviously, the piecewise-synchronous-modulation strategy is the most important and difficult part in the whole modulation strategy [8,9], but the synchronous modulation strategy (the ratio of f_s/f_c must be a constant integer) for the ESTPI is still a research gap.

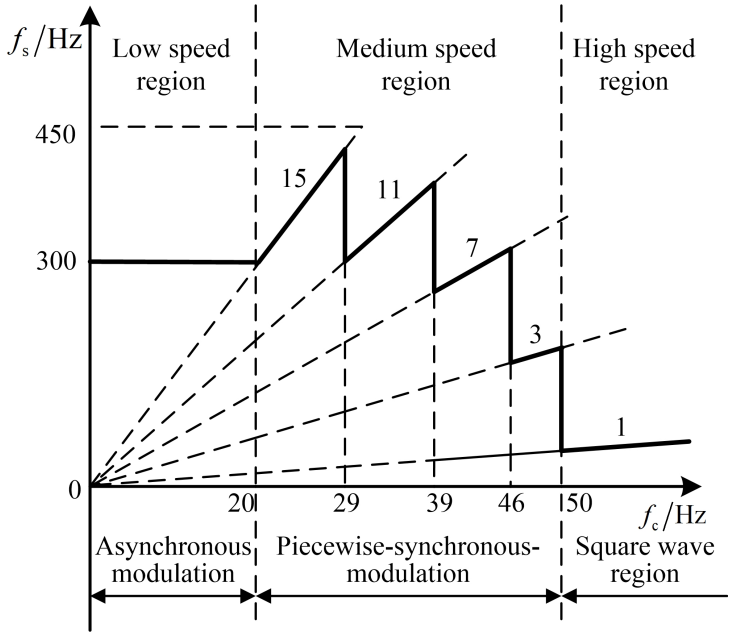

FIGURE 1. Multi-mode PWM strategy

The conventional synchronous modulation for 3L-NPC inverter can be classified into non-optimal synchronous modulation and optimal synchronous modulation [10-16]. Owing to the absence of some available voltage vectors caused by the lack of a controllable leg, the non-optimal synchronous modulation for the ESTPI can be hardly implemented. The current harmonic minimum PWM (CHMPWM) and the selective harmonic elimination PWM (SHEPWM) are two of the most popular optimal synchronous modulation strategies. Compared with the CHMPWM, the SHEPWM has the advantages listed as follows: the calculation of switching angles is simpler, the switching angles have continuous solutions during the whole modulation region, and the calculation accuracy of switching angles is not affected by the load parameters.

Consequently, the output harmonics of the ESTPI under synchronous modulation are analyzed firstly, in contrast with the conventional 3L-NPC inverter. Then, the SHEPWM based synchronous modulation strategy for the ESTPI is studied in this paper to improve the output voltage performance of the 3L-NPC inverter under fault-tolerant operation. Simulation results are presented to verify the proposed modulation strategy.

2. **Harmonic Analysis of ESTPI under Synchronous Modulation.** The fault-tolerant topology of 3L-NPC inverter is shown in Figure 2(a). Assuming that there is a fault in leg a, the leg a should be cut off to prevent the deterioration of system behavior. Connecting the output of leg a to the neutral point "O" by activating the bidirectional thyristor T_a, the post-fault topology can be simplified to the ESTPI, which is shown in Figure 2(b).

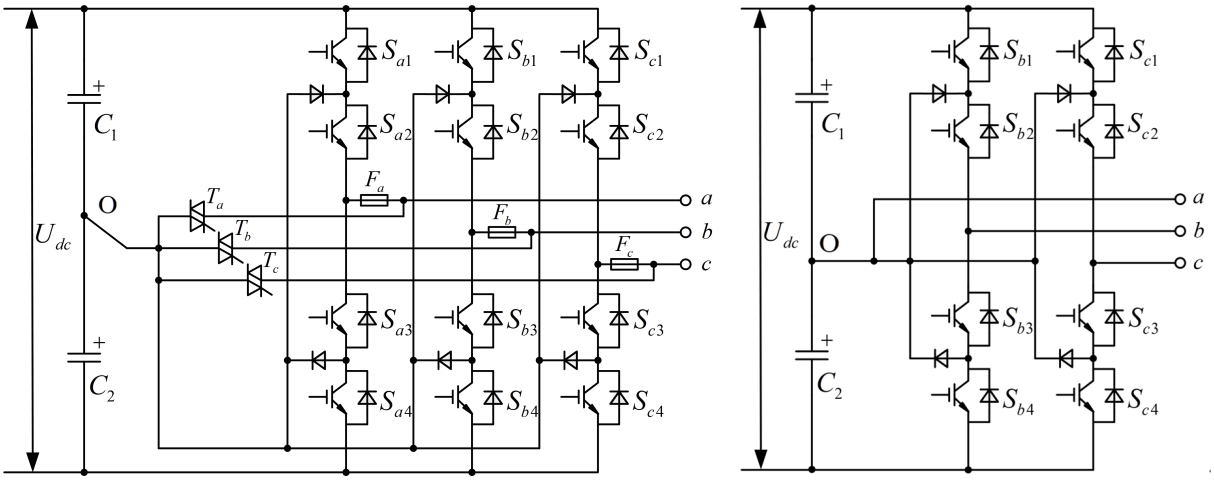

(a) Pre-fault topology (b) Post-fault topology

FIGURE 2. Topology of eight-switch three-phase inverter

In the post-fault topology, the leg a can only output level "0", so the three-phase pole voltage $u_{x\mathrm{O}}$ $(x = a, b, c)$ can be expressed in (1)

$$\begin{cases} u_{a\mathrm{O}} = 0 \\ u_{b\mathrm{O}} = A\sin(\omega t + \theta_1) \\ u_{c\mathrm{O}} = A\sin(\omega t + \theta_2) \end{cases} \tag{1}$$

where A is the amplitude of the pole voltage, and θ_1 and θ_2 are the initial phases of $u_{b\mathrm{O}}$ and $u_{c\mathrm{O}}$ respectively.

Accordingly, the three-phase fundamental line-to-line voltage of the ESTPI u_{xy} ($x = a, b, c$, $y = a, b, c$, and $x \neq y$) is derived as

$$\begin{cases} u_{ab} = u_{a\mathrm{O}} - u_{b\mathrm{O}} = A\sin(\omega t + \theta_1 + \pi) \\ u_{bc} = u_{b\mathrm{O}} - u_{c\mathrm{O}} = 2A\sin\dfrac{\theta_1 - \theta_2}{2}\sin\left(\omega t + \dfrac{\theta_1 + \theta_2}{2} + \dfrac{\pi}{2}\right) \\ u_{ca} = u_{c\mathrm{O}} - u_{a\mathrm{O}} = A\sin(\omega t + \theta_2) \end{cases} . \tag{2}$$

To ensure the balance of three-phase voltage, the amplitude of each line-to-line voltage should be equivalent, and the phase difference should be equal to $2\pi/3$, that is

$$2\sin\frac{\theta_1 - \theta_2}{2} = 1 \tag{3}$$

$$\begin{cases} \dfrac{\theta_1 - \theta_2}{2} + \dfrac{\pi}{2} = \dfrac{2\pi}{3} + 2k\pi \\ \theta_2 - \theta_1 - \pi = \dfrac{2\pi}{3} + 2k\pi \end{cases} \text{ or } \begin{cases} \dfrac{\theta_1 - \theta_2}{2} + \dfrac{\pi}{2} = -\dfrac{2\pi}{3} + 2k\pi \\ \theta_2 - \theta_1 - \pi = -\dfrac{2\pi}{3} + 2k\pi \end{cases} \quad (k \in N). \tag{4}$$

It can be deduced from the above expressions that the output voltage will satisfy the balanced condition when $\theta_1 - \theta_2 = \pi/3$, and the initial phase of the output voltage

changes by taking different values of θ_1 and θ_2. Specially, the three-phase fundamental line-to-neutral voltage u_{xn} $(x = a, b, c)$ takes phase a as reference, when $\theta_1 = -5\pi/6$ and $\theta_2 = -7\pi/6$, and can be written as

$$\begin{cases} u_{an} = \dfrac{A}{\sqrt{3}} \sin \omega t \\ u_{bn} = \dfrac{A}{\sqrt{3}} \sin\left(\omega t - 2\pi/3\right) \\ u_{cn} = \dfrac{A}{\sqrt{3}} \sin\left(\omega t + 2\pi/3\right) \end{cases} . \tag{5}$$

The three-phase modulation voltage, fundamental line-to-line voltage and fundamental line-to-neutral voltage of the ESTPI are shown in Figure 3, when $\theta_1 = -5\pi/6$ and $\theta_2 = -7\pi/6$.

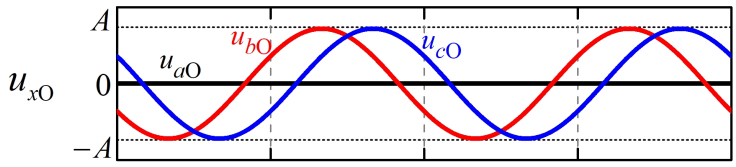

(a) Pole voltage

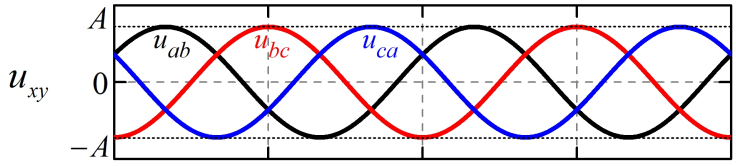

(b) Fundamental line-to-line voltage

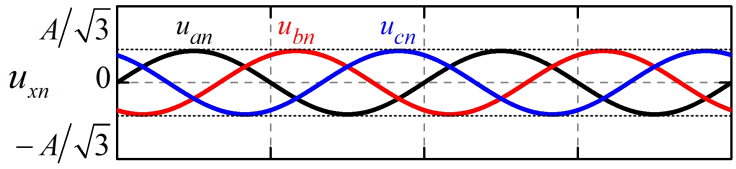

(c) Fundamental line-to-neutral voltage

FIGURE 3. Relationship among different voltages of ESTPI

Compared with asynchronous modulation, the synchronous modulation ensures that the output PWM pulses and the modulation voltage are strictly synchronous, in other words, the ratio of the carrier frequency to the output fundamental frequency must be an integer. Besides, the output PWM pulses must possess half-wave symmetry (HWS), quarter-wave symmetry (QWS) and three-phase symmetry (3PS) to reduce the output harmonics.

Due to the above symmetry, there are no even harmonics included in the output PWM pulses. The phase difference between the modulation voltages of the two controllable legs equals $\pi/3$ to guarantee the balance of the output voltage (taking $\theta_1 = -5\pi/6$ and $\theta_2 = -7\pi/6$ as an example). The three-phase pole voltage of ESTPI under synchronous modulation can be written as follows.

$$\begin{cases} u_{a\mathrm{O}} = 0 \\ u_{b\mathrm{O}} = \displaystyle\sum_{n=2k-1}^{\infty} A_n \sin\left[n\left(\omega t - \frac{5\pi}{6}\right)\right] \\ u_{c\mathrm{O}} = \displaystyle\sum_{n=2k-1}^{\infty} A_n \sin\left[n\left(\omega t - \frac{7\pi}{6}\right)\right] \end{cases} \quad (k = 1, 2, 3, \ldots). \tag{6}$$

The three-phase line-to-line voltage is obtained as

$$\begin{cases} u_{ab} = \displaystyle\sum_{n=2k-1, n\neq 3k}^{\infty} \left[A_n \sin\left(n\left(\omega t + \frac{\pi}{6}\right)\right)\right] + \sum_{n=2k-1, n=3k}^{\infty} \left[A_n \sin\left(n\left(\omega t - \frac{\pi}{2}\right)\right)\right] \\ u_{bc} = \displaystyle\sum_{n=2k-1, n\neq 3k}^{\infty} \left[A_n \sin\left(n\left(\omega t - \frac{\pi}{2}\right)\right)\right] - 2\sum_{n=2k-1, n=3k}^{\infty} \left[A_n \sin\left(n\left(\omega t - \frac{\pi}{2}\right)\right)\right] \\ u_{ca} = \displaystyle\sum_{n=2k-1, n\neq 3k}^{\infty} \left[A_n \sin\left(n\left(\omega t - \frac{7\pi}{6}\right)\right)\right] + \sum_{n=2k-1, n=3k}^{\infty} \left[A_n \sin\left(n\left(\omega t - \frac{\pi}{2}\right)\right)\right] \end{cases} \tag{7}$$

$(k = 1, 2, 3, \ldots)$.

According to the relationship between the line-to-line voltage and the line-to-neutral voltage, the three-phase line-to-neutral voltage can be derived as

$$\begin{cases} u_{an} = \dfrac{2}{3} \displaystyle\sum_{n=2k-1, n\neq 3k}^{\infty} \left[A_n \sin\left(n\left(\omega t + \frac{\pi}{2}\right)\right) \sin\left(n\left(-\frac{\pi}{3}\right)\right)\right] \\ u_{bn} = \dfrac{2}{3} \displaystyle\sum_{n=2k-1, n\neq 3k}^{\infty} \left[A_n \sin\left(n\left(\omega t - \frac{\pi}{6}\right)\right) \sin\left(n\left(-\frac{\pi}{3}\right)\right)\right] \\ \qquad - \displaystyle\sum_{n=2k-1, n=3k}^{\infty} \left[A_n \sin\left(n\left(\omega t - \frac{\pi}{2}\right)\right)\right] \\ u_{cn} = \dfrac{2}{3} \displaystyle\sum_{n=2k-1, n\neq 3k}^{\infty} \left[A_n \sin\left(n\left(\omega t - \frac{7\pi}{6}\right)\right) \sin\left(n\left(-\frac{\pi}{3}\right)\right)\right] \\ \qquad + \displaystyle\sum_{n=2k-1, n=3k}^{\infty} \left[A_n \sin\left(n\left(\omega t - \frac{\pi}{2}\right)\right)\right] \end{cases} . \tag{8}$$

It can be concluded from (7) and (8) that the output voltage of the ESTPI only includes the odd harmonics under synchronous modulation. Furthermore, the line-to-line voltages still include the frequency tripling harmonics with different amplitudes. The line-to-neutral voltages u_{bn} and u_{cn} also have the frequency tripling harmonics with equal amplitudes, while u_{an} has no frequency tripling harmonics.

Considering the different harmonic distribution of the output voltage in the ESTPI under synchronous modulation, the SHEPWM for the conventional 3L-NPC inverter is no longer applicable to the ESTPI. Hence, the SHEPWM for the ESTPI will be restudied in the following section, in order to eliminate the frequency tripling harmonics.

3. **Establishment and Solution of Nonlinear Equations of SHEPWM for ESTPI.** The output PWM pulse is shown in Figure 4(b). It satisfies the Dirichlet condition and its Fourier series expansion is written in (9).

$$u_{x\mathrm{O}}(\alpha) = \frac{a_0}{2} + \sum_{n=1}^{\infty} (a_n \cos n\alpha + b_n \sin n\alpha) \quad (x = b, c) \tag{9}$$

where

$$\begin{cases} a_0 = \dfrac{1}{\pi} \displaystyle\int_0^{2\pi} u_{x\mathrm{O}}(\alpha) \mathrm{d}\alpha \\ a_n = \dfrac{1}{\pi} \displaystyle\int_0^{2\pi} u_{x\mathrm{O}}(\alpha) \cos(n\alpha) \mathrm{d}\alpha \qquad (n = 1, 2, 3, \ldots). \\ b_n = \dfrac{1}{\pi} \displaystyle\int_0^{2\pi} u_{x\mathrm{O}}(\alpha) \sin(n\alpha) \mathrm{d}\alpha \end{cases} \tag{10}$$

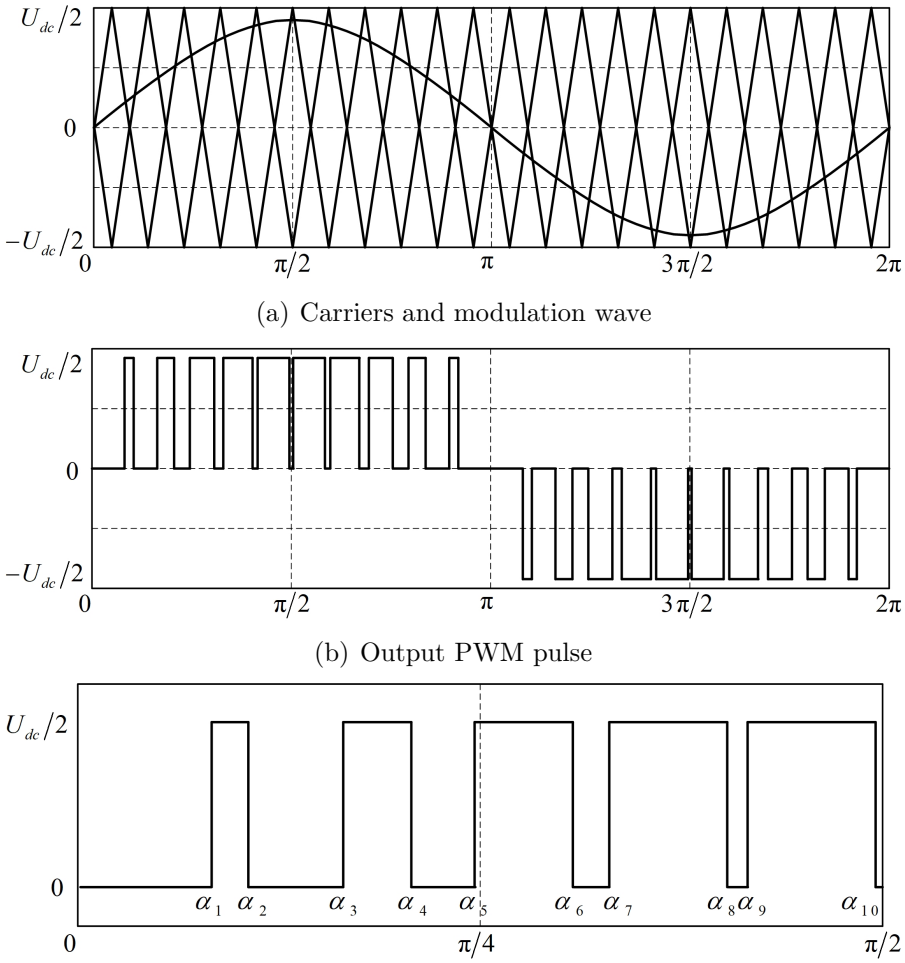

(a) Carriers and modulation wave

(b) Output PWM pulse

(c) Switching angles

FIGURE 4. Three-level synchronous modulation waveform and switching angle definition

On the basis of the symmetry of the output PWM pulse, it can be proved that $a_0 = a_n = 0$, and $b_n = 0$ when n is even. Accordingly, (9) can be simplified as

$$u_{x\mathrm{O}}(\alpha) = \sum_{n=1,3,5,\ldots}^{\infty} b_n \sin n\alpha \quad (x = b, c). \tag{11}$$

Combining Figure 4(b) and (10), b_n can be expressed as

$$b_n = \frac{2U_{dc}}{n\pi} \sum_{k=1}^{N} \left[(-1)^{k-1} \cos n\alpha_k\right] \quad (n = 1, 3, 5, \ldots) \tag{12}$$

where α_k is the switching angle, and N is the number of switching angles. The definition of α_k when $N = 10$ is shown in Figure 4(c), and the satisfied constraint condition of α_k is listed as

$$0 \le \alpha_1 < \alpha_2 < \alpha_3 < \cdots < \alpha_N \le \pi/2. \tag{13}$$

The objective of the SHEPWM is to find a set of α_k, making the amplitude of the output fundamental voltage equal the given value and eliminating the specific low-order harmonics. To eliminate $N-1$ low-order harmonics, α_k must satisfy the following conditions:

$$\begin{cases} \dfrac{2U_{dc}}{\pi} \displaystyle\sum_{k=1}^{N} \left[(-1)^{k-1} \cos \alpha_k\right] = U_{x\mathrm{O}} \\ \dfrac{2U_{dc}}{n\pi} \displaystyle\sum_{k=1}^{N} \left[(-1)^{k-1} \cos n\alpha_k\right] = 0 \end{cases} \quad (n = 3, 5, 7, \ldots, 2N-1) \tag{14}$$

where $U_{x\mathrm{O}}$ is the amplitude of the pole voltage. The relationship between $U_{x\mathrm{O}}$ and U_r is $U_{x\mathrm{O}} = \sqrt{3}U_r$, where U_r is the given value of the fundamental line-to-neutral voltage. After defining the modulation index of the ESTPI as $m = 2\sqrt{3}U_r/U_{dc}$, (14) can be rewritten as follows.

$$\begin{cases} \displaystyle\sum_{k=1}^{N} \left[(-1)^{k-1} \cos \alpha_k\right] = \frac{\pi}{4} m \\ \displaystyle\sum_{k=1}^{N} \left[(-1)^{k-1} \cos n\alpha_k\right] = 0 \end{cases} \quad (n = 3, 5, \ldots, 2N-1). \tag{15}$$

Therefore, (13) and (15) are the nonlinear equations of the SHEPWM for the ESTPI. It should be noted that the equations at $n = 3k$ $(k = 1, 2, 3, \ldots)$ are additionally added to eliminate the frequency tripling harmonics for the ESTPI.

Generally speaking, the output voltage harmonics decrease as the value of N increases. However, the equivalent carrier frequency of the inverter raises up simultaneously. In engineering applications, the carrier frequency of the inverter is usually limited to reduce switching loss, so the value of N is also limited and satisfied $N \le 15$ in most occasions. When $N = 10$, and $N = 11$, the equations of the SHEPWM for the ESTPI are listed as follows.

$$\begin{cases} \cos\alpha_1 - \cos\alpha_2 + \cos\alpha_3 - \cos\alpha_4 + \cdots + \cos\alpha_9 - \cos\alpha_{10} = \pi m/4 \\ \cos 3\alpha_1 - \cos 3\alpha_2 + \cos 3\alpha_3 - \cos 3\alpha_4 + \cdots + \cos 3\alpha_9 - \cos 3\alpha_{10} = 0 \\ \cos 5\alpha_1 - \cos 5\alpha_2 + \cos 5\alpha_3 - \cos 5\alpha_4 + \cdots + \cos 5\alpha_9 - \cos 5\alpha_{10} = 0 \\ \qquad\qquad\qquad\qquad \vdots \\ \cos 19\alpha_1 - \cos 19\alpha_2 + \cos 19\alpha_3 - \cos 19\alpha_4 + \cdots + \cos 19\alpha_9 - \cos 19\alpha_{10} = 0 \end{cases} \tag{16}$$

$$\begin{cases} \cos\alpha_1 - \cos\alpha_2 + \cos\alpha_3 - \cos\alpha_4 + \cdots - \cos\alpha_{10} + \cos\alpha_{11} = \pi m/4 \\ \cos 3\alpha_1 - \cos 3\alpha_2 + \cos 3\alpha_3 - \cos 3\alpha_4 + \cdots - \cos 3\alpha_{10} + \cos 3\alpha_{11} = 0 \\ \cos 5\alpha_1 - \cos 5\alpha_2 + \cos 5\alpha_3 - \cos 5\alpha_4 + \cdots - \cos 5\alpha_{10} + \cos 5\alpha_{11} = 0 \\ \qquad\qquad\qquad\qquad \vdots \\ \cos 21\alpha_1 - \cos 21\alpha_2 + \cos 21\alpha_3 - \cos 21\alpha_4 + \cdots - \cos 21\alpha_{10} + \cos 21\alpha_{11} = 0 \end{cases} \tag{17}$$

It can be seen that (16) and (17) are a set of nonlinear transcendental equations composed of trigonometric functions, whose partial derivatives can be easily obtained. Thus, the Newton iterative method is an effective method to solve the equations. However, the Newton iterative method is sensitive to the initial values, and the inappropriate initialization of iterative values may even cause the non-convergence of the iteration. The setting of the initial switching angles α_k for the SHEPWM will be discussed as follows.

The SVPWM and the CBPWM are the most commonly used modulation methods for the ESTPI. By contrast, the output PWM pulses of the ESTPI have a better symmetry and lower harmonics using the CBPWM strategy. Therefore, the switching angles in the CBPWM can be used for the initial values of that in the SHEPWM under the same conditions. Considering the HWS and QWS of the output PWM pulses, the phase opposition disposition PWM is most applicable to calculating the initial switching angle values of the SHEPWM, where the carriers and the modulation wave are shown in Figure 4(a). Besides, the relationship between the carrier frequency f_s and the modulation frequency f_c in the CBPWM is $f_s = (2N+2)f_c$. The initial values of the switching angles are shown in Table 1 and Table 2, at $m = 0.9$, $N = 10$ and $m = 0.9$, $N = 11$, respectively.

TABLE 1. Comparison between initial value and iteration result of the switching angles ($m = 0.9$, $N = 10$)

Switching angles	α_1	α_2	α_3	α_4	α_5
Initial value (°)	15.48	18	30.78	35.46	46.26
Iteration result (°)	13.62	17.28	27.42	34.62	41.62
Switching angles	α_6	α_7	α_8	α_9	α_{10}
Initial value (°)	52.74	61.92	69.66	77.94	86.4
Iteration result (°)	52.12	56.54	70.11	72.71	89.04

TABLE 2. Comparison between initial value and iteration result of the switching angles ($m = 0.9$, $N = 11$)

Switching angles	α_1	α_2	α_3	α_4	α_5	α_6
Initial value (°)	14.4	16.38	28.44	32.4	42.66	48.24
Iteration result (°)	12.66	15.77	25.45	31.57	38.54	47.48
Switching angles	α_7	α_8	α_9	α_{10}	α_{11}	
Initial value (°)	57.06	63.72	71.64	79.02	86.4	
Iteration result (°)	52.12	63.66	66.53	80.47	82.34	

Combining (16), (17), and the obtained initial switching angles, we can solve the nonlinear transcendental Equations (16) and (17) by the Newton iterative method. The iteration results are also listed in Table 1 and Table 2. It can be seen that the iteration results are close to the obtained initial values. Better initial values will greatly reduce the number of iterations with the Newton iterative method.

By changing the modulation index m, we can also calculate a class of solutions of Equations (16) and (17) at $N = 10$ and $N = 11$. The curves of the switching angles changing with the modulation index m are shown in Figure 5 at $N = 10$ and $N = 11$.

4. **Simulation Results.** To verify the effectiveness of the proposed SHEPWM method for the ESTPI, the simulation experiments are accomplished in MATLAB/Simulink. The simulation parameters are listed as follows: $U_{dc} = 500$V, $f_c = 50$Hz, $m = 0.7$, $R = 20\Omega$, and $L = 0.2$mH (RL load).

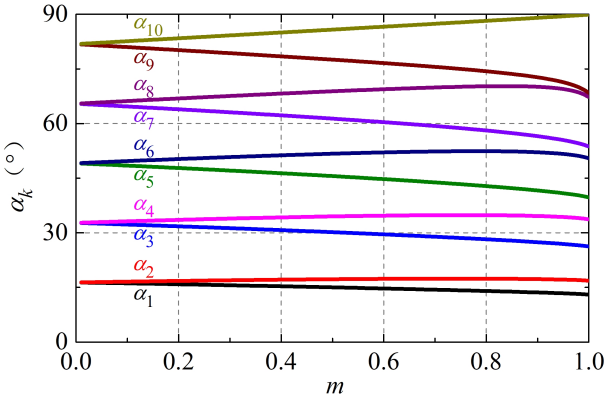

(a) $N = 10$

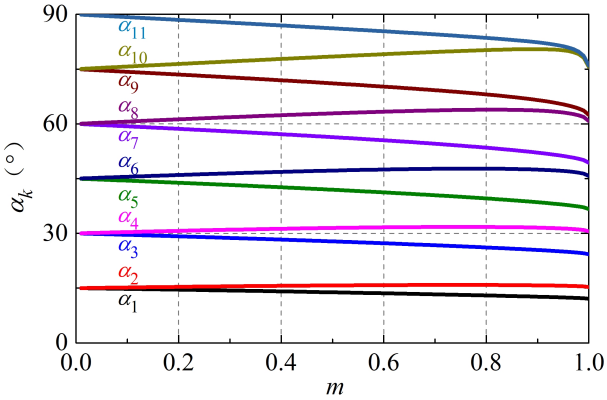

(b) $N = 11$

FIGURE 5. Curves of the switching angles changing with modulation index

When $N = 10$, the simulation results are shown in Figure 6. Theoretically, the SHEPWM method can eliminate 9 kinds of low-order harmonics for the ESTPI, namely, the 3rd, 5th, 7th, 9th, 11th, 13th, 15th, 17th, and 19th order harmonics. The simulation results show that the proposed SHEPWM method indeed eliminates the selective harmonics, and the amplitude of the fundamental line-to-line voltage is approximately equal to the given value $U_{line} = mU_{dc}/2 = 175$V. Moreover, the harmonic with maximum amplitude is the 21st harmonic when $N = 11$. The *THD* (Total Harmonic Distortion) of u_{bc} is far greater than that of u_{ab} and u_{ca}, since the amplitude of the frequency tripling harmonics in u_{bc} is twice as much as that in u_{ab} and u_{ca}. Considering that there is no frequency tripling harmonics in i_a, the *THD* of i_a is far less than that of i_b and i_c. This situation will happen at $N = 3k - 2$ $(k = 1, 2, 3, \ldots)$.

The simulation results are shown in Figure 7 at $N = 11$. The proposed SHEPWM method indeed eliminates 10 kinds of selective harmonics, namely, the 3rd, 5th, 7th, 9th, 11th, 13th, 15th, 17th, 19th and 21st order harmonics. The amplitude of the fundamental line-to-line voltage is also approximately equal to the given value. Because the harmonic with maximum amplitude, the 23rd harmonic, is not a frequency tripling harmonic, the *THD* of u_{bc} is slightly greater than that of u_{ab} and u_{ca}, and the *THD* of i_a is slightly less than that of i_b and i_c. The harmonic distribution in voltages and currents complies with the theoretical analysis.

The data statistics of experiment results at $N = 10$ and $N = 11$ are shown in Table 3 and Table 4, respectively. First, the fundamental amplitudes of the output voltages

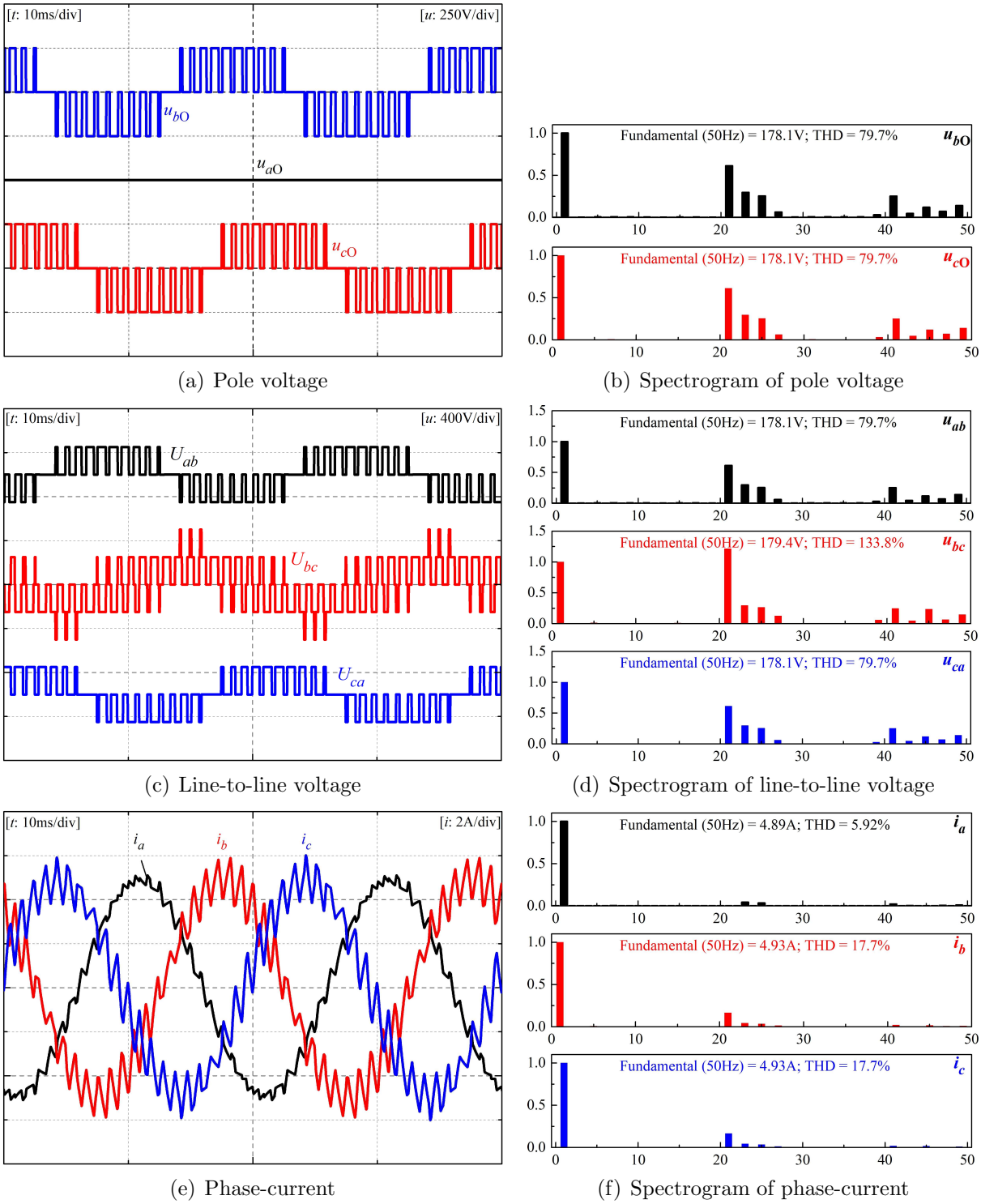

(a) Pole voltage (b) Spectrogram of pole voltage

(c) Line-to-line voltage (d) Spectrogram of line-to-line voltage

(e) Phase-current (f) Spectrogram of phase-current

FIGURE 6. Output waveforms and spectrograms of SHEPWM for ESTPI ($N = 10$)

approximately equal the theoretical value 175V, whatever N is. The proposed SHEPWM indeed eliminated the corresponding low-order harmonics. The highest order of the eliminated harmonics is 19 at $N = 10$, while the highest order of the eliminated harmonics is 21 at $N = 11$. Therefore, the proposed SHEPWM is demonstrated to be correct and effective. In addition, the greater N is, the less harmonic the output voltage contains,

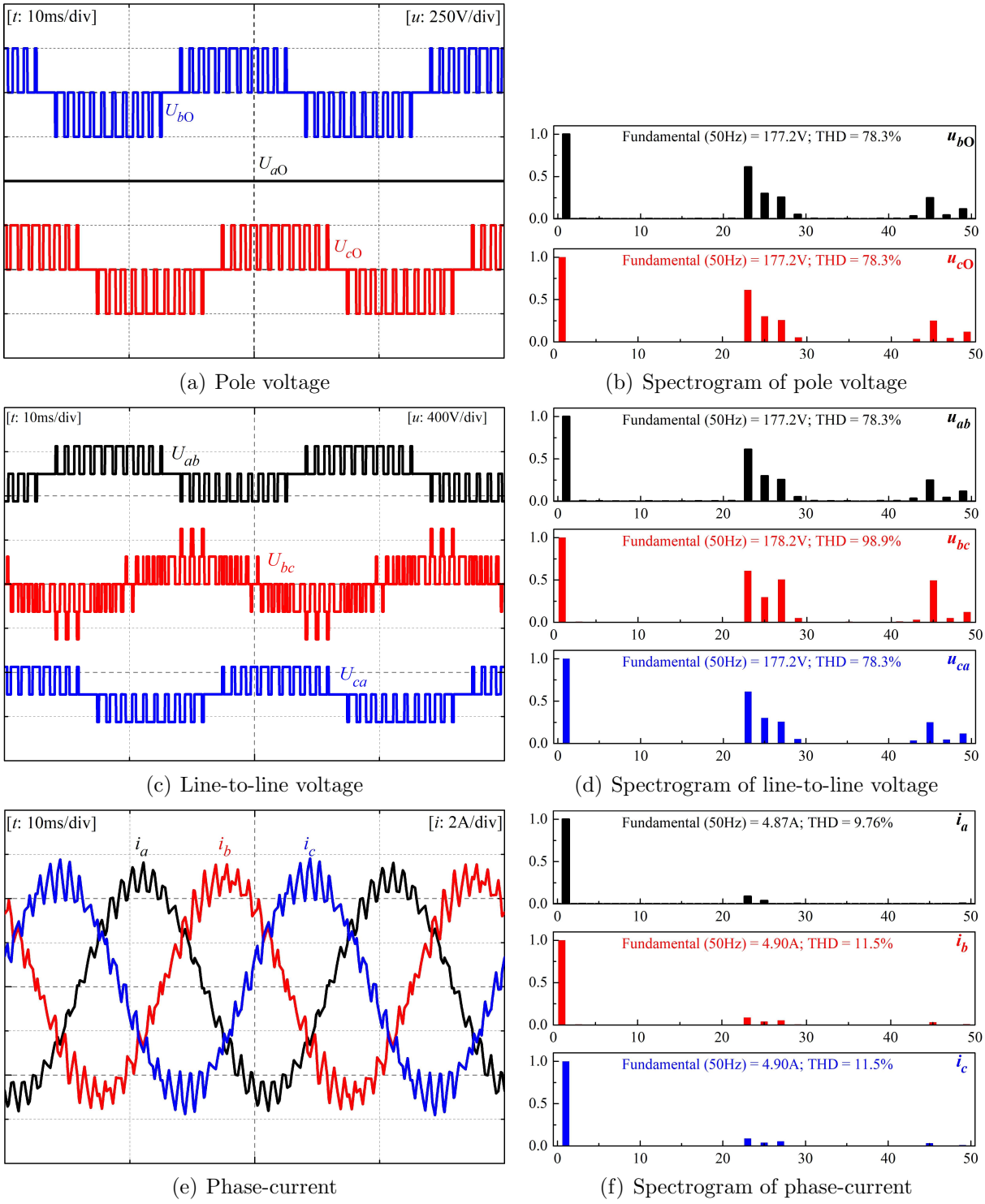

(a) Pole voltage (b) Spectrogram of pole voltage

(c) Line-to-line voltage (d) Spectrogram of line-to-line voltage

(e) Phase-current (f) Spectrogram of phase-current

FIGURE 7. Output waveforms and spectrograms of SHEPWM for ESTPI ($N = 11$)

which leads to a lower *THD* and makes the fundamental amplitude closer to the theoretical value. Specially, the harmonic distribution and *THD* will be changed a bit at $N = 3k - 2$ ($k = 1, 2, 3, \ldots$), which have negligible effect on the inverter performance, however.

TABLE 3. Data statistics of experiment result at $N = 10$

Parameter	Fundamental amplitude	*THD*	Lowest harmonic order
$u_{b\mathrm{O}}$	178.1V	79.7%	21
$u_{c\mathrm{O}}$	178.1V	79.7%	21
u_{ab}	178.1V	79.7%	21
u_{bc}	179.4V	133.8%	21
u_{ca}	178.1V	79.7%	21
i_a	4.89A	5.92%	23
i_b	4.93A	17.7%	21
i_c	4.93A	17.7%	21

TABLE 4. Data statistics of experiment result at $N = 11$

Parameter	Fundamental amplitude	*THD*	Lowest harmonic order
$u_{b\mathrm{O}}$	177.2V	78.3%	23
$u_{c\mathrm{O}}$	177.2V	78.3%	23
u_{ab}	177.2V	78.3%	23
u_{bc}	178.2V	98.9%	23
u_{ca}	177.2V	78.3%	23
i_a	4.87A	9.76%	23
i_b	4.90A	11.5%	23
i_c	4.90A	11.5%	23

It can be concluded from the above simulation results that the proposed ESTPI SHEPWM method indeed eliminates the selective low-order harmonics, including the frequency tripling harmonics, and also ensure that the amplitude of the output fundamental voltage is equal to the given value. The proposed method will improve the output performance of the 3L-NPC inverter under fault-tolerant operation control at low switching frequency, and is of great significance for high-power occasions asking for high safety and reliability, such as electric traction system, variable frequency speed regulation system, and flexible AC transmission system.

5. **Conclusion.** The eight-switch three-phase inverter (ESTPI) is chosen as the fault-tolerant topology of the 3L-NPC inverter, and the output harmonic of the ESTPI under synchronous modulation is firstly analyzed in this paper. It is proved that the line-to-line voltage and line-to-neutral voltage still have the frequency tripling harmonics with different amplitudes. To eliminate the low-order harmonics including the frequency tripling harmonics, the SHEPWM for the ESTPI is proposed in this paper. The simulation results show the effectiveness and feasibility of the proposed method. However, there are still several problems for the future research, such as the smooth switching process between different values of N in the piecewise-synchronous-modulation strategy.

Acknowledgment. This work is partially supported by the National Natural Science Foundation of China (grants 51377013 and 51407023). The authors also gratefully acknowledge the helpful comments and suggestions of the reviewers, which have improved the presentation.

REFERENCES

[1] Y. Song, X. Li and W. Cai, Adaptive and fault-tolerant reactive power compensation in power systems via multilevel STATCOMs, *International Journal of Innovative Computing, Information and Control*, vol.9, no.8, pp.3403-3413, 2013.

[2] G. Chen and J. Kang, Universal formulations and computation algorithm for three-phase space vector PWM ripple current analysis, *International Journal of Innovative Computing, Information and Control*, vol.14, no.2, pp.587-602, 2018.

[3] S. Li and L. Xu, Strategies of fault tolerant operation for three-level PWM inverters, *IEEE Trans. Power Electron.*, vol.21, no.4, pp.933-940, 2006.

[4] G.-T. Park, T.-J. Kim, D.-W. Kang and D.-S. Hyun, Control method of NPC inverter for continuous operation under one phase fault condition, *Conference Record of the 39th IEEE IAS Annual Meeting*, pp.2188-2193, 2004.

[5] B. R. Lin and T. C. Wei, Space vector modulation strategy for an eight-switch three-phase NPC converter, *IEEE Trans. Aerosp. Electron. Syst.*, vol.40, no.2, pp.553-566, 2004.

[6] P. Lezana, J. Pou, T. A. Meynard et al., Survey on fault operation on multilevel inverters, *IEEE Trans. Ind. Electron.*, vol.57, no.7, pp.2207-2218, 2010.

[7] Y. C. Liu, X. L. Ge, X. Y. Feng et al., Relationship between SVPWM and carrier-based PWM of eight-switch three-phase inverter, *Electron. Lett.*, vol.51, no.13, pp.1018-1019, 2015.

[8] C. Wang, K. Wang and X. You, Research on synchronized SVPWM strategies under low switching frequency for six-phase VSI-fed asymmetrical dual stator induction machine, *IEEE Trans. Ind. Electron.*, vol.63, no.11, pp.6767-6776, 2016.

[9] K. Wang, X. J. You, C. C. Wang et al., Research on synchronized SVPWM strategies under low switching frequency, *Proc. of the CSEE*, vol.35, no.16, pp.4175-4183, 2015.

[10] R. J. Ding, Features of 60° SPWM control and its circuit realization, *Electric Drive for Locomotives*, no.1, pp.13-17, 1995.

[11] C. Wang, M. Zhou and X. You, Research on the PWM method of high power AC electrical locomotive, *Transactions of China Electrotechnical Society*, vol.27, no.2, pp.173-178, 2012.

[12] G. Narayanan and V. T. Ranganathan, Two novel synchronized bus-clamping PWM strategies based on space vector approach for high power drives, *IEEE Trans. Power Electron.*, vol.17, no.1, pp.84-93, 2002.

[13] K. Dong, Hybrid pulse width modulation strategy based on current harmonic minimum technique, *Transactions of China Electrotechnical Society*, vol.32, no.20, pp.179-188, 2017.

[14] Z. Zhang, X. Ge, Z. Tian et al., A PWM for minimum current harmonic distortion in metro traction PMSM with saliency ratio and load angle constrains, *IEEE Trans. Power Electron.*, vol.33, no.5, pp.4498-4511, 2018.

[15] S. Ahmad, I. Ashraf, A. Iqbal et al., SHEPWM for multilevel inverter using modified NR and pattern generation for wide range of solutions, *Proc. of the 12th IEEE Conf. on Compatibility, Power Electronics & Power Engineering*, pp.1-6, 2018.

[16] M. A. Memon, S. Mekhilef and M. Mubin, Selective harmonic elimination in multilevel inverter using hybrid APSO algorithm, *IET Power Electron.*, vol.11, no.10, pp.1673-1680, 2018.